The evolution of hydrogen induced defects and the restoration of π-plasmon as a monitor of the thermal reduction of graphene oxide

Gianluca Di Filippo[a], Andrea Liscio[b], Alessandro Ruocco[a,*]

[a] *Dipartimento di Scienze, Università degli Studi Roma Tre, via della Vasca Navale 84, 00146 Rome (Italy)*
[b] *Consiglio Nazionale delle Ricerche, Istituto per la Microelettronica e Microsistemi (CNR-IMM), viale del Fosso del Cavaliere 100, 00133 Rome (Italy)*

Abstract

In this paper, we study the modification of the optical, chemical and electronic properties of graphene oxide (GO) during thermal reduction in ultra-high-vacuum by combining the results of several electron spectroscopies. We find that the fraction of oxygen moieties on the surface, as deduced from the evolution of C 1s core level in photoemission, is progressively reduced upon increasing the annealing temperature from 150 to 650 °C. The intensity of the CH stretching mode, associated with CH defects on GO surface and measured in the low energy region of electron energy loss spectra (EELS), decreases as a function of the annealing temperature. The removal or the reduction of such hydrogen or oxygen defects induces a restoration of sp^2 carbon hybridization. The presence of such hybridization is confirmed by the capability to excite π-plasmon as observed in the EELS spectra. In particular we find a critical annealing temperature (T_{ann} = 300 °C) at which π-plasmon excitation via electron scattering is accessible suggesting the formation of graphene-like domains with size comparable with the plasmon wavelength ($\lambda_p \sim 5$ nm). The linear dispersion of π-band close to Fermi level, as measured in UPS, confirms the formation of graphene-like domains.

Keywords: graphene oxide, thermal reduction, electronic properties, CH defects, π-plasmon, electron energy loss spectroscopy

*Corresponding author
Email address: alessandro.ruocco@uniroma3.it (Alessandro Ruocco)

1. Introduction

Graphene oxide (GO) is a very promising material due to its water solubility enabling solution processing. Alternative industrial deposition methods such as inkjet printing [1] or gravure printing [2] have been recently applied in GO processing. GO is a purely 2D composite materials given by an insulating matrix (containing: sp^3 carbons, grain boundaries, defects, holes, oxygen functional groups, etc.) and a conductive filler given by the sp^2 domains (a.k.a. nanographene). The relative amount of the filler and as well as the composition of the matrix play a crucial role in the chemico-physical properties of the single sheet. In particular, the electrical properties can be tuned by varying the degree of oxidation or reduction. Pristine GO is an electrical insulator and the electrical conductivity can be partially brought to a form closer to defective pristine graphene called reduced graphene oxide (rGO) via effective removal of oxygen moieties by chemical [3] and/or thermal [4, 5] treatment. Such intrinsic structural complexity reflects on its wide range of properties and applications reported in literature, for example GO/rGO are used as functional electronic sensors [3, 6] and in energy and environmental applications [7, 8, 9]. Moreover, the abundance of chemical functionalities in GO makes these sheets a highly versatile chemical platform for creating new graphene-based materials.

Despite the large efforts devoted in studying the mechanisms involved in GO reduction and the role of defects, a comprehensive analysis of the optical properties of such materials is still lacking. Due to structural and energetical disorder, the quantitative analysis of Raman spectra of rGO is not straightforward as in the case of pristine graphene, even if several efforts have been devoted using quantitative statistical analysis [10].

In this paper, we study the thermal annealing processes by monitoring in-situ the modification of the optical, chemical and electronic properties during the thermal reduction of GO in ultra-high vacuum (UHV) using a dedicated home-made electron spectrometer. In particular, we examine the electron energy loss spectra (EELS) in the vibrational (< 1 eV) and collective excitation region (up to 30 eV of loss) and the evolution of C 1s core level and the valence band via photoemission spectroscopy. Electron spectroscopies are high-surface sensitive techniques and can be successfully used to monitor single sheets, thin-films and coatings allowing to distinguish the contribution of the GO from the substrate one. The use of thermal annealing

provides high reproducibility and, in particular, does not introduce any contaminant, as is the case for chemical reduction [11].

The structure of GO is usually assumed to be a graphene sheet bonded to oxygen in the form of hydroxyl and epoxy groups with a very small contribution of carbonyl and carboxyl groups, which predominantly decorate the edges of the sheets. Despite the huge effort to understand the structural and morphological properties of GO, a coherent and detailed description of its structure and of the reduction process has not yet been achieved. For example, many models do not take into consideration the presence of CH defects at the surface and only predict hydrogen atoms to be part of hydroxyl and carboxyl groups [12], nonetheless graphene can react with atomic hydrogen especially when its structure is defective as in the case of GO [13]. In addition, the effects of GO reduction on the build-up of the collective oscillation of the electrons in the π-states, i.e. the π-plasmon, have been rarely discussed. From this point of view EELS is a powerful surface sensitive technique able to gives information on the presence and the evolution of CH defects and the restoration of π-plasmon in the thermal reduction of GO. CH-defects on graphitic surfaces are known to change carbon hybridization from sp^2 to sp^3 transforming conducting systems into insulators[13]. On the contrary the π-plasmon is one of the typical fingerprints of conductive graphitic structures. Its characteristic energy in the long wavelength limit and in pure carbon allotrope with sp^2 structure, ranges from 4.7 eV in free standing graphene [14] to 6.5 eV in graphite in specular reflection [15] passing for 5.1 eV for single wall carbon nano tube (SWCNT) [16]. The reduction of the excitation energy of π-plasmon moving from bulk graphite to 2D graphene is associated to the reduction of the screening and to the interlayer coupling [17]. The same mechanisms play an important role in the π-plasmon energy when graphene is grown on different metal and semiconductor substrates. For instance a typical value close to that of π-plasmon in graphite is found in the graphene/Pt(111) (6.2 eV)[18], in this case the variation of the plasmon energy is attributed to the screening of the substrate. In the case of graphene/Ni(111) interface the plasmon energy is found at 7.5 eV [19]. Here, the π-plasmon energy shift respect to the pristine graphene is the consequence of the strong band structure changes of the graphene layer, due to the interaction between graphene and the Ni substrate. A different behaviour is found in the graphene/SiC(0001) [20], in this case the π-plasmon energy for the single epi-

taxial graphene layer is 5.1 eV close to the suspended graphene and its energy increases as a function of the number of graphene layers. In these cases, as a consequence of the weak interaction, the effective response function can be obtained as the sum of the distinct response functions of graphene and the substrate [21]. Moreover, its excitation probability is extremely sensitive to the presence of foreign species [22]. The build-up of such a collective mode can be only observed if well ordered, defect-free sp^2 domains are available on the surface. Therefore, the spatial extension of the plasmon is a characteristic length that could be related to the minimum size of graphitic domains. A deeper understanding of the role of CH-defects and the behaviour of the π-plasmon upon thermal treatment is essential to fully understand the mechanisms behind GO reduction. These two arguments are the main point dealt with in this work.

2. Experimental methods

2.1. Sample preparation

GO sheets were produced by a modified Hummers method [23], centrifuged, dispersed in water (concentration = 1.5 g L^{-1}) and spin-coated (1500 rpm) on p-doped Si(110) (ρ=0.005 Ω·cm) covered by 2 nm thick native silicon oxide layer (SiO_x). The lateral size of the GO sheets is 428±14 nm. Mean value and standard error are calculated by statistical analysis performed on $>$ 3000 sheets [24].

SiO_x substrates were cleaned by sonication in acetone bath followed by ozone treatment for 30 minutes and a final rinsing in 2-propanol. The GO thermal reduction was performed in ultra-high-vacuum (UHV) by annealing the samples at four temperatures: 150, 300, 500 and 650 °C, for 5 minutes. After every annealing, the sample was cooled at room temperature (RT). A low rate heating ramp was used ($\sim$ 10 °C/min) in order to ensure efficient removal of oxygen functional groups with minimum carbon losses.

2.2. Morphological characterization

AFM measurements were performed under ambient conditions at $\sim$ 10% relative humidity by blowing a gentle flow of N_2 in the chamber containing the microscope and RT with a scanning raster rate of 1 Hz. The AFM images were recorded using a Multimode IIIa (Bruker)

scanning probe microscope, equipped with the Extender Electronics Module, in tapping mode using a MPP-11100 probe (Bruker, Si with frequency = 270 KHz and nominal tip radius of about 10 nm).

Quantitative analysis was performed by applying the threshold filter to the corresponding histogram analysis [25] on 10 AFM images for a total sampled surface of about 1000 μm^2. The measured height of the sheets amounts to 8±2 Å in agreement with previous results [4] where the variance corresponds to the sheet roughness.

2.3. Electronic characterization

All experiments were performed at room temperature in an UHV chamber with a base pressure of 3×10^{-10} mbar. The system is equipped with several surface science techniques. X-ray and UV photoelectron spectroscopy (XPS, UPS) and electron energy loss spectroscopy (EELS) were used in this study. For XPS a monochromatized OMICRON Al K_α source ($h\nu$ = 1486.7 eV) was used. The excitation source for UPS was a He-discharge lamp ($h\nu$ = 21.2 eV and 40.8 eV). Electrons were detected by means of a hemispherical energy analyzer equipped with a channeltron. The energy resolution of the analyzer corresponds to 1.5 % of the pass energy. The overall energy resolution (source + analyzer) was 0.5 eV and 0.2 eV for XPS and UPS, respectively. A home-built monochromatic electron source (described in Ref. 26) was used for electron energy loss measurements. EELS spectra were taken in specular geometry at a primary beam energy of 90.75 eV with grazing angle of 30°. The energy resolution (full width at half maximum) of the incoming electron beam corresponds to 0.05 eV. A Faraday cup was mounted close to the sample position to monitor the incident current ($170 \div 220$ pA). Spectra were acquired in the energy loss range $E_L \leq 30$ eV with an energy resolution of 0.2 eV. The vibrational properties of the samples were additionally investigated via acquiring EELS spectra close to the elastic peak ($E_L \leq 1$ eV) with an overall energy resolution of 0.06 eV.

2.4. Fitting procedures

According to current literature, the C 1s spectrum of pristine GO contains six contributions which are commonly associated with carbon atoms in different configuration and chemical environment [27, 28]. From lower to higher binding energy they correspond to: sp^2-carbon, sp^3-carbon, C-OH and C-O-C, C=O and COOH. The deconvolution of the C 1s spectra of rGO

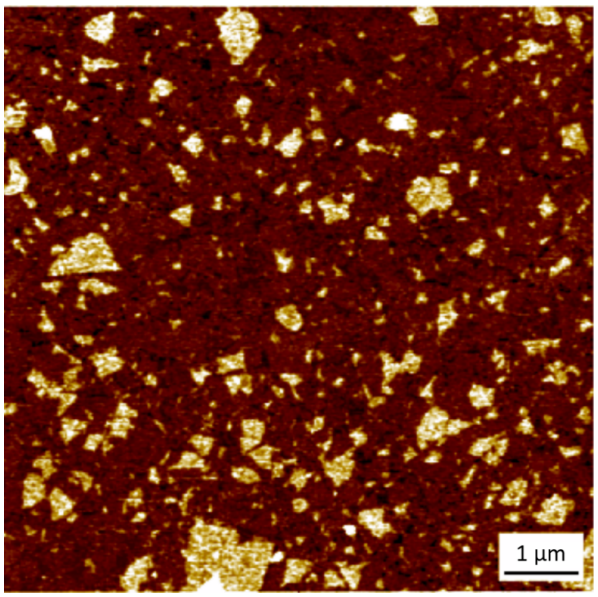

Figure 1: Topographic AFM image of GO ultra-thin film. Dark (light) brown regions represent single (double) sheets of GO. Black spots correspond to bare SiO_x substrate. Z-range = 2 nm.

(shown in section 3.1) was obtained by using five peaks and a Shirley type integral background. Voigt profiles were used in the fitting procedure except for the sp^2 contribution peak that was fitted with a Doniach-Sunjic curve. The asymmetry value calculated by the best fit amounts to $\alpha = 1.1 \pm 0.1$ at all annealing temperatures. This value is in excellent agreement with the asymmetry value measured on graphite [29]. An analogous procedure (Voigt profiles + Shirley background) was used to reproduce the vibrational part of the electron energy loss spectra (section 3.3).

3. Results and discussion

The experimental setup and the aim of the study provide two requirements: i) the used electron spectroscopies are not lateral resolved techniques, and the surface area sampled by the electronic spot amounts to few mm^2 and ii) we want to prevent the interaction of the sp^2 clusters inter-GO sheets. For this reason, we enhanced the contribution of the single GO sheets preparing ultra-thin GO films with controlled morphology on macroscopic scale (about 1 cm^2) by minimizing both the area of the bare SiO_x and the formation of multi-sheets or multilayers. Figure 1 shows a representative AFM image of the sample surface morphology

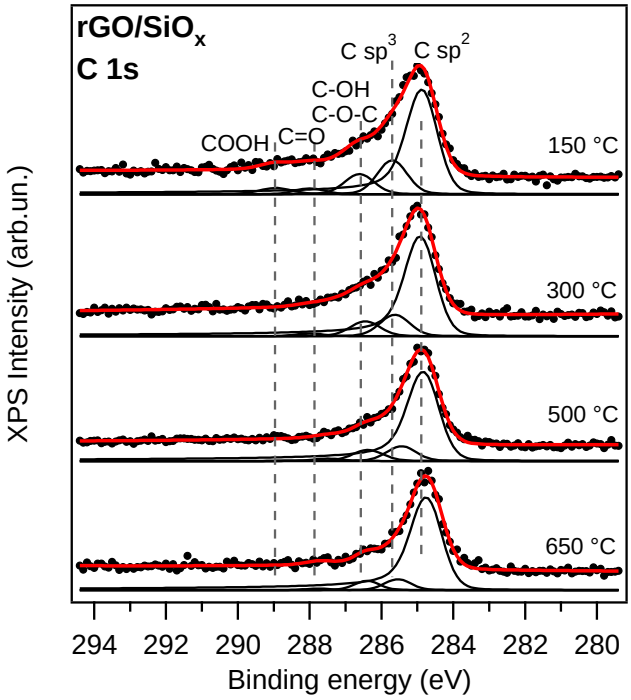

Figure 2: C 1s surveys of rGO at different T_{ann}. Components related to different carbon species are indicated by the thin solid lines. The thick line represents the best fit to the experimental data.

where SiO_x substrate and GO sheets can be unambiguously distinguished having different color corresponding to different height. Due to the high affinity with the substrate GO tends to cover the silicon surface (bare $SiO_x < 3\%$) forming a uniform patchwork of single sheets ($80 \pm 1\%$ of coverage) a second layer of isolated sheets ($16 \pm 2\%$) and further higher layers ($< 1\%$).

3.1. Chemical analysis (XPS measurements)

The quantitative analysis of the reduction degree has been done by monitoring the evolution of the core-level photoemission signal as a function of the annealing temperature (T_{ann}) from 150 °C to 650 °C (all the results are summarized in Table 3.1). Figure 2 shows the C 1s XPS lines of rGO acquired at increasing T_{ann}. As expected, sp^2 hybridization ($E_b = 284.8$ eV) is the most intense component for all T_{ann} values. At 150 °C the C 1s line of rGO shows four additional features associated with defects and oxygen functional groups. The peak at $E_b = 285.7$ eV is associated with C in sp^3 hybridization. It is well known that in graphene

T_{ann} (°C)	sp^2 (±0.03)	sp^3 (±0.01)	C-OH & C-O-C (±0.01)	C=O (±0.01)	COOH (±0.01)	sp^3/sp^2
150	0.68	0.15	0.10	0.04	0.03	0.22
300	0.76	0.12	0.09	0.02	0.01	0.16
500	0.81	0.10	0.07	0.01	0.01	0.12
650	0.86	0.08	0.06	0.01	–	0.09

Table 1: Relative abundance of the carbon species present on rGO, obtained from the fits shown in figure 2. The sp^3 to sp^2 ratio quantifies the degree of GO reduction

oxide the presence of oxygen groups leads to a distortion of the graphitic sp^2 network and to the formation of tetrahedral bonds [30]. Thus, the ratio of the intensity of the sp^3 component to the sp^2 one is a suitable tool to determine the degree of GO reduction (right column in Tab. 3.1). The peak at E_b = 286.6 eV contains the unresolved contributions of hydroxide (C-OH) and epoxide (C-O-C). Carbonyl (C=O) is observed at E_b = 287.9 eV and carboxyl (COOH) at E_b = 288.9 eV. The sp^2 carbon line accounts for 68% of the total spectral weight, while the remaining intensity is mostly due to sp^3 defects (15%) and epoxy and hydroxyl groups (10%). According to current models describing the atomic structure of GO [30, 31] COOH and C=O species are bound to sp^2 carbon and decorate the edges of the GO sheets. They can be easily removed upon thermal reduction explaining why the amount of those species (4% COOH and 3% C=O) is rather small already at the lowest annealing temperature. Upon annealing at 300 °C COOH and C=O species are almost entirely removed ($\sim$ 3% of the total spectral weight) and only C-OH and C-O-C groups (9%), together with sp^3 defects (12%) are left on the surface. Hydroxyl and epoxy groups form a covalent bond with sp^3 hybridized carbon and a higher temperature is needed to remove those groups. At 500 and 650 °C most of the spectral weight ($>$ 80%) is associated with sp^2 (graphene-like) carbon. The signal from oxidized ($\sim$ 5%) and defected sites ($\sim$ 7%) is detectable even at the highest reduction temperature.

3.2. Valence band analysis (UPS measurements)

The valence-band properties of rGO were studied using UPS. Figure 3(a) shows the evolution of the valence-band-photoemission spectrum with the annealing temperature. He II

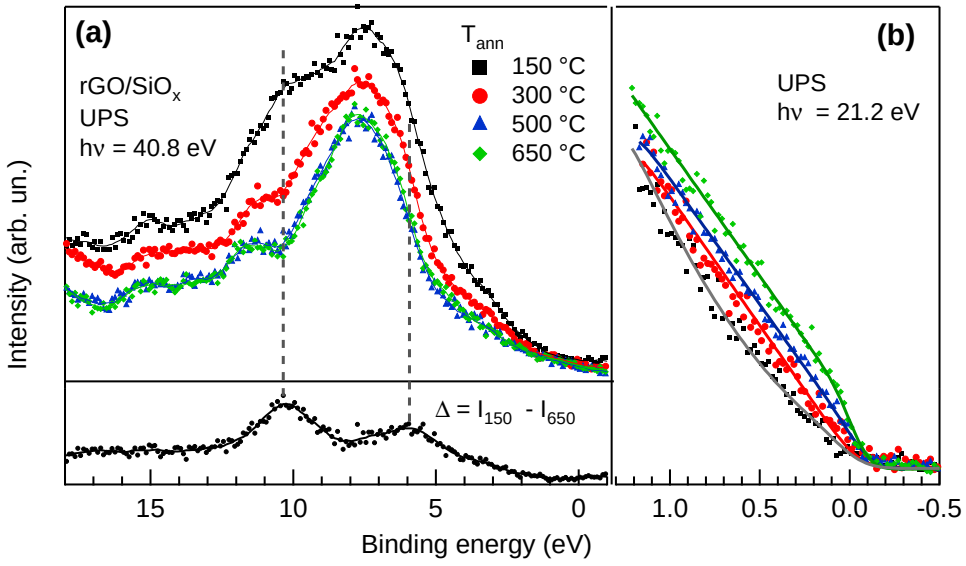

Figure 3: Photoemission of rGO annealed at different T_{ann}. (a) Valence band photoemission spectra (the solid lines are guide to the eye). (inset) Point by point difference (Δ) between the spectra acquired at T_{ann} = 150 °C and 650 °C. (b) Spectral region near the Fermi level. The solid lines are polynomial fitting curves.

radiation (hν = 40.8 eV) was used in order to reduce the background of secondary electrons and obtain better resolved curves. The largest evolution of the valence band line is obtained upon annealing at 300 °C, while no appreciable differences are observed when the annealing temperature is increased from 500 °C to 650 °C. All the spectra are dominated by a broad band centered at $E_b \sim 7.5$ eV. This structure is associated with the emission of electrons from the bottom of the π-band near the Γ point of graphene. Further contributions from the top σ-band close to the M-point can also be observed [32]. With the increasing of T_{ann}, the main structure becomes sharper. Such evidence can be ascribable to the presence of further contributions of oxygen functional groups decreasing during the reduction, located at 6 and 10.5 eV, respectively and corresponding to O 2p and C 2p states in epoxy and carbonyl groups [33, 34]. The two contributions are clearly evinced in the inset of figure 3(a), as reported by the point-by-point difference between the spectra measured at the lower and higher T_{ann}: $\Delta = I_{150} - I_{650}$. The decreasing of the signal related to the oxygen levels reflects to a variation of the density of states (DOS) near the Fermi energy, as evinced in the evolution of the line-shape of the UPS spectra (measured with He-I radiation) for different T_{ann}, as reported

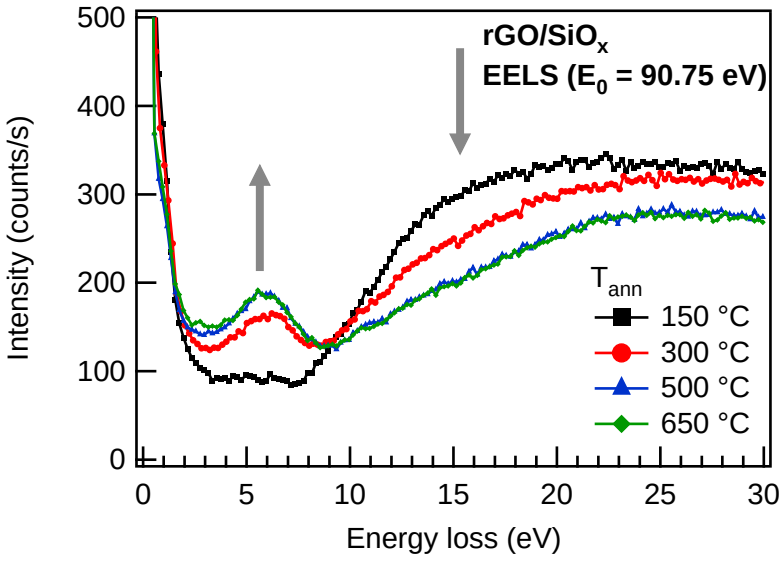

Figure 4: EELS spectra acquired at different annealing temperature.

in Figure 3(b). We reproduced the measured line-shapes using as fitting function the product of a polynomial (describing the DOS) and the Fermi distribution. For $T_{ann} \geq 300$ °C DOS is linear, being characteristic of the π-states in graphene where the line slope is inversely proportional to the square of the Fermi velocity [35]. It is noteworthy to underline that the slope does not depend on T_{ann}, strongly suggesting that reduction does not affect the Fermi velocity in the π-states. Focusing the analysis near the E_F, we achieve an increasing of the DOS with T_{ann}, corresponding to a metallic behavior due to the doping effect of the substrate, as previously observed in graphene/SiO_2 [36, 37].

3.3. Electronic and vibrational excitations (EELS measurements)

The reduction also affects the behavior of the electronic excitations, as evinced by monitoring the characteristic loss features acquired by EELS shown in Figure 4. The most evident variation is observed between 150 °C and 300 °C. A well distinguished peak at 6 eV is achieved at $T_{ann} \geq 300$ °C, while at the lower temperature it is hardly discernible from the background. Correspondingly, a decreasing of a broad structure, located between 10 eV and 30 eV is observed. The latter corresponds to collective modes and electronic transitions involving the combined π and σ electrons (i.e. $\pi + \sigma$ plasmon). In the first stages of the

reduction ($T_{ann} \leq 500$ °C) the EELS intensity in the energy region centered around 15 eV decreases. Such feature corresponds to GO transitions due to epoxy, hydroxyl and carbonyl functional groups [38]. At $T_{ann} \geq 500$ °C only a broad structure centered around 24 eV remains, corresponding to $\pi + \sigma$ plasmon.

The loss peak centered at $\sim$ 6 eV is given by the characteristic π-plasmon excitation of graphene [14, 39] (i.e. the collective in-phase oscillation of electrons in π states), representing the fingerprint of the presence of long-range-ordered sp^2 regions. The π-plasmon energy is larger than the one observed in free-standing graphene of 4.7 eV [14]. Similar shift it has been observed in several graphene/metal interfaces both in case of strong interaction (graphene/Ni(111) [19]) or even in case of weak interaction (graphene/Pt(111) [18]). In the latter the screening of the substrate plays a fundamental role in the variation of plasmon energy at the interface [21]. It has been established that the interaction between graphene and SiO_2 is essentially via van der Waals forces [40], as a consequence the shift of π-plasmon energy measured in rGO, with respect to the pristine graphene, is ascribable to the screening of the substrate. Besides, cannot be excluded that a minimal part of this energy shift is related to an increasing of the electron density due to the doping effect of the substrate [41], in agreement with our UPS analysis.

By increasing T_{ann} the amount of sp^2 carbon only varies from 68% to 76%, as measured by XPS (Tab. 3.1). It is noteworthy to highlight the build-up of the π-plasmon despite the limited increase in the percentage of sp^2 carbon. In general, the build-up of the self-sustaining π-plasmon oscillation is determined not simply by the concentration of sp^2 C atoms, but also on their organization (i.e. the size and order of the graphene-like regions) [42, 43]. Thus, we can distinguish two contributions affecting the π-plasmon oscillation: lateral size of sp^2 regions, presence of defects and oxygen groups. The latter can be selectively located along the sp^2 regions: epoxy and hydroxyl groups are mainly attached to the basal plane while carboxyl group are mainly at the boundaries. DFT calculations have shown that a favorable configuration is reached when those groups aggregate together to form extended structures [44] given by graphene-like parts surrounded by fully-oxidized sp^3-carbon regions, as showed by TEM measurements [45]. Additional studies suggested that pristine GO consists of $\sim$ 3 nm sp^2 clusters embedded within a sp^3 carbon matrix [6, 46] (figure 5 left). Being the lateral dimension

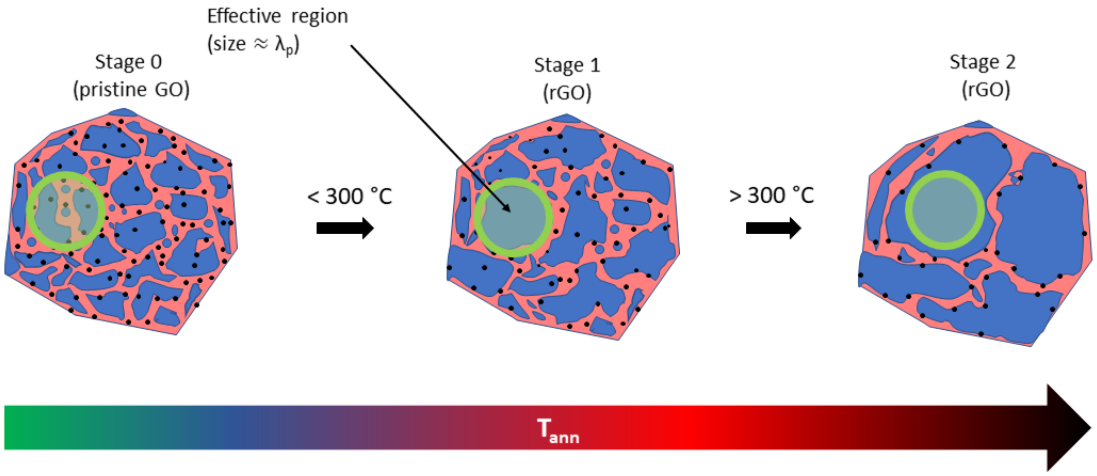

Figure 5: schematic view of the reduction process of GO. Blue regions correspond to sp^2 domains, red regions to disordered and oxidized areas, black dots represent defects (e.g. CH_n).

of the graphitic domains smaller than the wavelength of the plasmon field investigated in the EELS experiment ($\lambda_p \sim 5$ nm) [47], we are not able to excite the selected π-plasmon unless larger sp^2 domains are formed upon reduction. At $T_{ann} = 300$ °C the formation of small sp^2 domains results in the merging of the larger sp^2 clusters and in the formation of graphitic areas larger than λ_p, allowing the excitation of the π-plasmon (figure 5 center). Once sp^2 domains large enough to sustain the plasmon oscillation are formed the intensity of the plasmon loss is only marginally affected by an additional increase of the reduction temperature (figure 5 right).

In addition to the effect of the size and defects due to oxygen functional groups, another important class of defects is related to distortion of the aromatic bond and holes filled by hydrogen (CH functional groups). Due to the broad line of the C 1s signal, a detailed analysis of CH functional groups cannot be performed by XPS alone. However, EELS (with appropriate energy resolution) can provide a direct insight to the vibrational properties of the system. With our apparatus we have access to vibrational modes involving carbon atoms. Figure 6 shows the evolution of the EELS spectrum of rGO for different T_{ann} within the loss energy region $E_L < 1$ eV ($E_L < 8000$ cm^{-1}). The measured spectra show several loss structures whose intensities decrease with increasing T_{ann} strongly suggesting that such features are related to

oxygen functional groups and defects.

The vibrational properties of rGO have been extensively studied over the years by means of IR-spectroscopy [48, 49, 50]. Excitations in the energy range $120^{\smile} - 135$ meV were attributed to C-C and C-O skeletal modes. The energy resolution of the EELS measurements does not allow to separate those two contributions that are therefore observed as the single broad structure at 129 meV. The portion of the spectrum corresponding to energy loss larger than 150 meV is magnified. The sharp peak located at 355 meV corresponds to CH stretching bands (ν_{CH}). The corresponding overtone is observed at 715 meV ($2\nu_{CH}$). In addition to the CH bands a broad energy loss feature appears at $\sim$ 470 meV. Many IR-spectroscopy studies showed the presence of a broad and intense vibrational band in the energy region from 350 to 500 meV that was associated with the OH stretching (ν_{OH}) of C-OH, COOH groups and H_2O molecules [49, 50]. The latter are very abundant due to the high humidity content of graphene oxide [50]. The presence of such a strong band obscures the IR-signal coming from CH defects and make the analysis of their evolution with the reduction temperature very complicated. This is one of the reasons why most of the structural models of GO do not consider the presence of CH bonds. In the EELS spectra shown in this work the ν_{CH} contribution dominates over the OH one and allows to get a new insight on such defects. In the first annealing step (from 150 to 300 °C) the amount of CH groups is reduced by nearly 50%. The intensity drops to 25% upon 500 °C annealing and an additional decreasing is achieved at $T_{ann} = 650$ °C reaching to 12% of the starting value. It cannot be excluded that part of CH defects are the result of water dissociation at room temperature during the sample preparation. This process is similar to what occur to graphene grown on metal substrate and exposed to water [51]. Independently from the origin of such defects, it is clear that the annealing reduces their presence of almost a factor 10 with respect the starting value.

Additional information can be obtained via looking at the energy position of the peaks. For T_{ann} up to 500 °C the CH-stretch energy is found at 355 ± 4 meV revealing that most of the hydrogen atoms are bound to carbon atoms in tetrahedral configuration forming sp^3 CH_n ($n = 1; 2; 3$) complexes [52] in the basal plane, as observed in hydrogenated graphene where the carbon hybridization changes from sp^2 to sp^3 [13]. At 650 °C the position of the ν_{CH} peak shifts in the characteristic range of sp^2 CH stretch [52] at 372 ± 5 meV suggesting

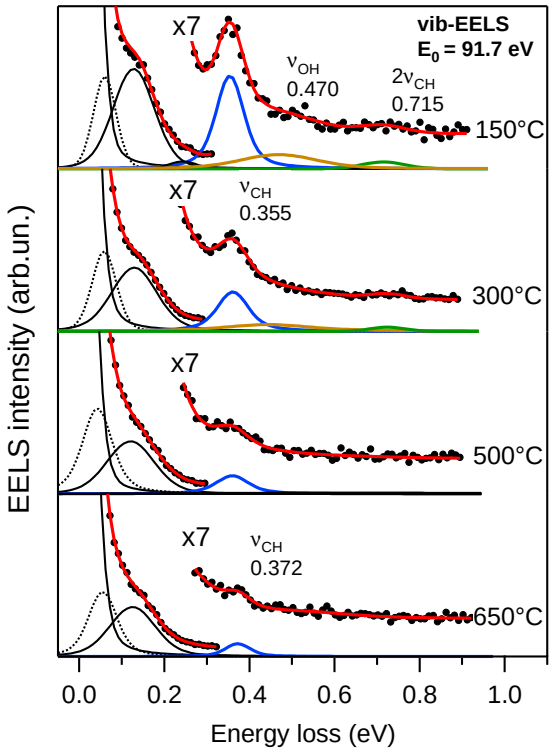

Figure 6: EELS spectra acquired at different annealing temperature. The measured curves (circles) are fitted with Voigt functions (thin solid lines). The thick solid lines represent the best fits to the spectra.

that the remaining hydrogen is decorating the edges of the graphene domains. At this T_{ann} an additional contribution of holes and carbon vacancies (generated in the annealing process) filled with hydrogen atoms cannot be excluded [53].

4. Conclusions

In this work we showed that the use of electron spectroscopies (XPS, UPS and EELS) provides a quantitative in-situ characterization of the structural, electronic and optical properties of GO reduced by thermal treatment. In particular, EELS allows to investigate the localization and the evolution of CH defects and to investigate the restoration of the π-plasmon typical of carbon network in sp^2 hybridization.

As well known, the thermal reduction promotes the desorption of oxygen functional groups allowing the restoration of the sp^2 network and the corresponding decreasing of distorted sp^3

carbon atoms. The corresponding electronic states due to the functional groups at $6-11$ eV of binding energy disappear, while a linear dispersion of the π-bands emerges near the Fermi level. It is evident that XPS measurements alone is not able to give informations on the dimension of the sp^2 hybridization region and only the combination of XPS with other electron spectroscopies provides this morphological information. In particular, the presence of the π-plasmon, as revealed in EELS, is an indication of the growth of the lateral dimensions of the sp^2 graphitic islands over 5 nm for T_{ann} above 300 °C.

An accurate analysis of the CH stretching mode reveals the presence of CH defects in sp^2 and sp^3 hybridization region located at the edges and on the basal plane, respectively. Heating at 650 °C provides to remove CH defects in the sp^3 region, while CH defects associated with the sp^2 region are left and decorate the edges of the graphene-like domains to saturate dangling bonds.

5. Acknowledgements

The research leading to these results has received funding from the European Union's Horizon 2020 research and innovation programme under GrapheneCore2 785219 (Graphene Flagship). Partial financial support by Universitá Roma Tre, "Piano Straordinario della Ricerca 2015, azione n. 3 -Potenziamento dei laboratori di ricerca- " is greatly acknowledged.

References

[1] P. He, B. Derby, Inkjet printing ultra-large graphene oxide flakes, 2D Mater. 4 (2) (2017) 021021. doi:10.1088/2053-1583/aa629e.
URL https://doi.org/10.1088/2053-1583/aa629e

[2] E. B. Secor, S. Lim, H. Zhang, C. D. Frisbie, L. F. Francis, M. C. Hersam, Gravure Printing of Graphene for Large-area Flexible Electronics, Adv. Mater. 26 (26) (2014) 4533–4538. doi:10.1002/adma.201401052.
URL https://onlinelibrary.wiley.com/doi/abs/10.1002/adma.201401052

[3] S. Gilje, S. Han, M. Wang, K. L. Wang, R. B. Kaner, A Chemical Route to Graphene for

Device Applications, Nano Lett. 7 (11) (2007) 3394–3398. doi:10.1021/nl0717715.
URL https://doi.org/10.1021/nl0717715

[4] A. Liscio, G. P. Veronese, E. Treossi, F. Suriano, F. Rossella, V. Bellani, R. Rizzoli, P. Samorì, V. Palermo, Charge transport in graphene-polythiophene blends as studied by Kelvin Probe Force Microscopy and transistor characterization, J. Mater. Chem. 21 (9) (2011) 2924–2931. doi:10.1039/C0JM02940H.
URL https://pubs.rsc.org/en/content/articlelanding/2011/jm/c0jm02940h

[5] R. Larciprete, S. Fabris, T. Sun, P. Lacovig, A. Baraldi, S. Lizzit, Dual Path Mechanism in the Thermal Reduction of Graphene Oxide, J. Am. Chem. Soc. 133 (43) (2011) 17315–17321. doi:10.1021/ja205168x.
URL https://doi.org/10.1021/ja205168x

[6] C. Gómez-Navarro, R. T. Weitz, A. M. Bittner, M. Scolari, A. Mews, M. Burghard, K. Kern, Electronic Transport Properties of Individual Chemically Reduced Graphene Oxide Sheets, Nano Lett. 7 (11) (2007) 3499–3503. doi:10.1021/nl072090c.
URL https://doi.org/10.1021/nl072090c

[7] C. Ogata, R. Kurogi, K. Awaya, K. Hatakeyama, T. Taniguchi, M. Koinuma, Y. Matsumoto, All-Graphene Oxide Flexible Solid-State Supercapacitors with Enhanced Electrochemical Performance, ACS Appl. Mater. Interfaces 9 (31) (2017) 26151–26160. doi:10.1021/acsami.7b04180.
URL https://doi.org/10.1021/acsami.7b04180

[8] Y. Wang, Z. Shi, Y. Huang, Y. Ma, C. Wang, M. Chen, Y. Chen, Supercapacitor Devices Based on Graphene Materials, J. Phys. Chem. C 113 (30) (2009) 13103–13107. doi:10.1021/jp902214f.
URL https://doi.org/10.1021/jp902214f

[9] F. Li, X. Jiang, J. Zhao, S. Zhang, Graphene oxide: A promising nanomaterial for energy and environmental applications, Nano Energy 16 (2015) 488–515. doi:10.1016/j.nanoen.2015.07.014.
URL http://www.sciencedirect.com/science/article/pii/S2211285515003079

[10] A. Wróblewska, A. Dużyńska, J. Judek, L. Stobiński, K. Żerańska, A. P. Gertych, M. Zdrojek, Statistical analysis of the reduction process of graphene oxide probed by Raman spectroscopy mapping, J. Phys.: Condens. Matter 29 (47) (2017) 475201. doi:10.1088/1361-648X/aa92fe.
URL http://stacks.iop.org/0953-8984/29/i=47/a=475201

[11] N. Mohanty, A. Nagaraja, J. Armesto, V. Berry, High-Throughput, Ultrafast Synthesis of Solution- Dispersed Graphene via a Facile Hydride Chemistry, Small 6 (2) (2010) 226–231. doi:10.1002/smll.200901505.
URL https://onlinelibrary.wiley.com/doi/abs/10.1002/smll.200901505

[12] S. Sajjad, S. A. Khan Leghari, A. Iqbal, Study of Graphene Oxide Structural Features for Catalytic, Antibacterial, Gas Sensing, and Metals Decontamination Environmental Applications, ACS Appl. Mater. Interfaces 9 (50) (2017) 43393–43414. doi:10.1021/acsami.7b08232.
URL https://doi.org/10.1021/acsami.7b08232

[13] D. C. Elias, R. R. Nair, T. M. G. Mohiuddin, S. V. Morozov, P. Blake, M. P. Halsall, A. C. Ferrari, D. W. Boukhvalov, M. I. Katsnelson, A. K. Geim, K. S. Novoselov, Control of Graphene's Properties by Reversible Hydrogenation: Evidence for Graphane, Science 323 (5914) (2009) 610–613. doi:10.1126/science.1167130.
URL http://science.sciencemag.org/content/323/5914/610

[14] T. Eberlein, U. Bangert, R. R. Nair, R. Jones, M. Gass, A. L. Bleloch, K. S. Novoselov, A. Geim, P. R. Briddon, Plasmon spectroscopy of free-standing graphene films, Phys. Rev. B 77 (23) (2008) 233406. doi:10.1103/PhysRevB.77.233406.
URL https://link.aps.org/doi/10.1103/PhysRevB.77.233406

[15] A. Ruocco, M. Milani, S. Nannarone, G. Stefani, Scattering mechanism of electrons interacting with surfaces in specular reflection geometry: Graphite, Physical Review B 59 (20) (1999) 13359–13364. doi:10.1103/PhysRevB.59.13359.

[16] C. Kramberger, R. Hambach, C. Giorgetti, M. H. Rümmeli, M. Knupfer, J. Fink, B. Büchner, L. Reining, E. Einarsson, S. Maruyama, et al., Linear plasmon dispersion in single-

wall carbon nanotubes and the collective excitation spectrum of graphene, Physical Review Letters 100 (19) (2008) 196803. doi:10.1103/PhysRevLett.100.196803.

[17] A. Politano, G. Chiarello, Plasmon modes in graphene: status and prospect, Nanoscale 6 (2014) 10927. doi:10.1039/C4NR03143A.
URL http://dx.doi.org/10.1039/C4NR03143A

[18] A. Politano, A. R. Marino, V. Formoso, D. Farías, R. Miranda, G. Chiarello, Quadratic dispersion and damping processes of π plasmon in monolayer graphene on pt(111), Plasmonics 7 (2) (2012) 369–376. doi:10.1007/s11468-011-9317-1.

[19] A. Generalov, Y. Dedkov, Eels study of the epitaxial graphene/ni(111) and graphene/au/ni(111) systems, Carbon 50 (1) (2012) 183–191. doi:10.1016/j.carbon.2011.08.018.

[20] J. Lu, K. P. Loh, H. Huang, W. Chen, A. T. S. Wee, Plasmon dispersion on epitaxial graphene studied using high-resolution electron energy-loss spectroscopy, Physical Review B 80 (11) (2009) 113410. doi:10.1103/PhysRevB.80.113410.

[21] J. Yan, K. S. Thygesen, K. W. Jacobsen, Nonlocal screening of plasmons in graphene by semiconducting and metallic substrates: First-principles calculations, Physical Review Letters 106 (14) (2011) 146803. doi:10.1103/PhysRevLett.106.146803.

[22] W. Cheung, M. Patel, Y. Ma, Y. Chen, Q. Xie, J. V. Lockard, Y. Gao, H. He, π-Plasmon absorption of carbon nanotubes for the selective and sensitive detection of Fe3+ ions, Chem. Sci. 7 (8) (2016) 5192–5199. doi:10.1039/C6SC00006A.
URL https://pubs.rsc.org/en/content/articlelanding/2016/sc/c6sc00006a

[23] E. Treossi, M. Melucci, A. Liscio, M. Gazzano, P. Samorì, V. Palermo, High-Contrast Visualization of Graphene Oxide on Dye-Sensitized Glass, Quartz, and Silicon by Fluorescence Quenching, J. Am. Chem. Soc. 131 (43) (2009) 15576–15577. doi:10.1021/ja9055382.
URL https://doi.org/10.1021/ja9055382

[24] A. Liscio, K. Kouroupis-Agalou, X. D. Betriu, A. Kovtun, Emanuele Treossi, N. M. Pugno, G. D. Luca, L. Giorgini, V. Palermo, Evolution of the size and shape of 2d nanosheets

during ultrasonic fragmentation, 2D Mater. 4 (2) (2017) 025017. doi:10.1088/2053-1583/aa57ff.
URL http://stacks.iop.org/2053-1583/4/i=2/a=025017

[25] A. Liscio, Scanning Probe Microscopy beyond Imaging: A General Tool for Quantitative Analysis, ChemPhysChem 14 (6) (2013) 1283–1292. doi:10.1002/cphc.201200880.
URL https://onlinelibrary.wiley.com/doi/abs/10.1002/cphc.201200880

[26] G. M. Pierantozzi, M. Sbroscia, A. Ruocco, Templating effect of the substrate on the structure of Cu-phthalocyanine thin film, Surface Science 669 (2018) 176–182. doi:10.1016/j.susc.2017.12.003.
URL http://www.sciencedirect.com/science/article/pii/S0039602817306647

[27] K. Haubner, J. Murawski, P. Olk, L. M. Eng, C. Ziegler, B. Adolphi, E. Jaehne, The Route to Functional Graphene Oxide, ChemPhysChem 11 (10) (2010) 2131–2139. doi:10.1002/cphc.201000132.
URL https://onlinelibrary.wiley.com/doi/abs/10.1002/cphc.201000132

[28] A. Kovtun, D. Jones, S. Dell'Elce, E. Treossi, A. Liscio, V. Palermo, Accurate chemical analysis of oxygenated graphene-based materials using X-ray photoelectron spectroscopy, Carbon 143 (2019) 268–275. doi:10.1016/j.carbon.2018.11.012.
URL http://www.sciencedirect.com/science/article/pii/S0008622318310297

[29] P. M. T. M. van Attekum, G. K. Wertheim, Excitonic Effects in Core-Hole Screening, Phys. Rev. Lett. 43 (25) (1979) 1896–1898. doi:10.1103/PhysRevLett.43.1896.
URL https://link.aps.org/doi/10.1103/PhysRevLett.43.1896

[30] A. Lerf, H. He, M. Forster, J. Klinowski, Structure of Graphite Oxide Revisited, J. Phys. Chem. B 102 (23) (1998) 4477–4482. doi:10.1021/jp9731821.
URL https://doi.org/10.1021/jp9731821

[31] W. Cai, R. D. Piner, F. J. Stadermann, S. Park, M. A. Shaibat, Y. Ishii, D. Yang, A. Velamakanni, S. J. An, M. Stoller, J. An, D. Chen, R. S. Ruoff, Synthesis and Solid-State NMR Structural Characterization of 13c-Labeled Graphite Oxide, Science 321 (5897)

(2008) 1815–1817. doi:10.1126/science.1162369.
URL http://science.sciencemag.org/content/321/5897/1815

[32] T. Ohta, A. Bostwick, J. L. McChesney, T. Seyller, K. Horn, E. Rotenberg, Interlayer Interaction and Electronic Screening in Multilayer Graphene Investigated with Angle-Resolved Photoemission Spectroscopy, Phys. Rev. Lett. 98 (20) (2007) 206802. doi:10.1103/PhysRevLett.98.206802.
URL https://link.aps.org/doi/10.1103/PhysRevLett.98.206802

[33] M. Lundie, Ž. Šljivančanin, S. Tomić, Electronic and optical properties of reduced graphene oxide, J. Mater. Chem. C 3 (29) (2015) 7632–7641. doi:10.1039/C5TC00437C.
URL https://pubs.rsc.org/en/content/articlelanding/2015/tc/c5tc00437c

[34] Q. Zhang, H. Zhang, X.-L. Cheng, Highly stable two-dimensional graphene oxide: Electronic properties of its periodic structure and optical properties of its nanostructures, Chin. Phys. B 27 (2) (2018) 027301. doi:10.1088/1674-1056/27/2/027301.
URL http://stacks.iop.org/1674-1056/27/i=2/a=027301?key=crossref.62331e7c9fbd79a540f35136

[35] A. H. Castro Neto, F. Guinea, N. M. R. Peres, K. S. Novoselov, A. K. Geim, The electronic properties of graphene, Rev. Mod. Phys. 81 (1) (2009) 109–162. doi:10.1103/RevModPhys.81.109.
URL https://link.aps.org/doi/10.1103/RevModPhys.81.109

[36] Y. Shi, X. Dong, P. Chen, J. Wang, L.-J. Li, Effective doping of single-layer graphene from underlying SiO_2 substrates, Phys. Rev. B 79 (11) (Mar. 2009). doi:10.1103/PhysRevB.79.115402.
URL https://link.aps.org/doi/10.1103/PhysRevB.79.115402

[37] S. D. Costa, J. E. Weis, O. Frank, M. Fridrichová, M. Kalbac, Monitoring the doping of graphene on SiO2/Si substrates during the thermal annealing process, RSC Adv. 6 (2016) 72859–72864.

[38] P. Johari, V. B. Shenoy, Modulating Optical Properties of Graphene Oxide: Role of

Prominent Functional Groups, ACS Nano 5 (9) (2011) 7640–7647. doi:10.1021/nn202732t.
URL https://doi.org/10.1021/nn202732t

[39] J. Lu, K. P. Loh, H. Huang, W. Chen, A. T. S. Wee, Plasmon dispersion on epitaxial graphene studied using high-resolution electron energy-loss spectroscopy, Phys. Rev. B 80 (11) (2009) 113410. doi:10.1103/PhysRevB.80.113410.
URL https://link.aps.org/doi/10.1103/PhysRevB.80.113410

[40] T. C. Nguyen, M. Otani, S. Okada, Semiconducting electronic property of graphene adsorbed on (0001) surfaces of sio 2, Physical Review Letters 106 (10) (2011) 106801. doi:10.1103/PhysRevLett.106.106801.

[41] S. Entani, Y. Matsumoto, M. Ohtomo, P. V. Avramov, H. Naramoto, S. Sakai, Precise control of single- and bi-layer graphene growths on epitaxial Ni(111) thin film, J. Appl. Phys. 111 (6) (2012) 064324. doi:10.1063/1.3694662.
URL https://aip.scitation.org/doi/10.1063/1.3694662

[42] M.-L. Theye, V. Paret, Spatial organization of the sp^2-hybridized carbon atoms and electronic density of states of hydrogenated amorphous carbon films, Carbon 40 (8) (2002) 1153–1166. doi:10.1016/S0008-6223(01)00291-3.
URL http://linkinghub.elsevier.com/retrieve/pii/S0008622301002913

[43] P. M. Ajayan, S. Iijima, T. Ichihashi, Electron-energy-loss spectroscopy of carbon nanometer-size tubes, Phys. Rev. B 47 (11) (1993) 6859–6862. doi:10.1103/PhysRevB.47.6859.
URL https://link.aps.org/doi/10.1103/PhysRevB.47.6859

[44] J.-A. Yan, L. Xian, M. Y. Chou, Structural and Electronic Properties of Oxidized Graphene, Phys. Rev. Lett. 103 (8) (2009) 086802. doi:10.1103/PhysRevLett.103.086802.
URL https://link.aps.org/doi/10.1103/PhysRevLett.103.086802

[45] K. Erickson, R. Erni, Z. Lee, N. Alem, W. Gannett, A. Zettl, Determination of the Local Chemical Structure of Graphene Oxide and Reduced Graphene Oxide, Adv. Mater.

22 (40) (2010) 4467–4472. doi:10.1002/adma.201000732.
URL http://doi.wiley.com/10.1002/adma.201000732

[46] C. Mattevi, G. Eda, S. Agnoli, S. Miller, K. A. Mkhoyan, O. Celik, D. Mastrogiovanni, G. Granozzi, E. Garfunkel, M. Chhowalla, Evolution of Electrical, Chemical, and Structural Properties of Transparent and Conducting Chemically Derived Graphene Thin Films, Adv. Funct. Mater. 19 (16) (2009) 2577–2583. doi:10.1002/adfm.200900166.
URL https://onlinelibrary.wiley.com/doi/abs/10.1002/adfm.200900166

[47] F. Moresco, M. Rocca, T. Hildebrandt, M. Henzler, Plasmon Confinement in Ultrathin Continuous Ag Films, Phys. Rev. Lett. 83 (11) (1999) 2238–2241. doi:10.1103/PhysRevLett.83.2238.
URL https://link.aps.org/doi/10.1103/PhysRevLett.83.2238

[48] C. Zhang, D. M. Dabbs, L.-M. Liu, I. A. Aksay, R. Car, A. Selloni, Combined Effects of Functional Groups, Lattice Defects, and Edges in the Infrared Spectra of Graphene Oxide, J. Phys. Chem. C 119 (32) (2015) 18167–18176. doi:10.1021/acs.jpcc.5b02727.
URL http://pubs.acs.org/doi/10.1021/acs.jpcc.5b02727

[49] M. Acik, G. Lee, C. Mattevi, A. Pirkle, R. M. Wallace, M. Chhowalla, K. Cho, Y. Chabal, The Role of Oxygen during Thermal Reduction of Graphene Oxide Studied by Infrared Absorption Spectroscopy, J. Phys. Chem. C 115 (40) (2011) 19761–19781. doi:10.1021/jp2052618.
URL http://pubs.acs.org/doi/10.1021/jp2052618

[50] T. Szabó, O. Berkesi, I. Dékány, DRIFT study of deuterium-exchanged graphite oxide, Carbon 43 (15) (2005) 3186–3189. doi:10.1016/j.carbon.2005.07.013.
URL http://linkinghub.elsevier.com/retrieve/pii/S0008622305004070

[51] A. Politano, M. Cattelan, D. W. Boukhvalov, D. Campi, A. Cupolillo, S. Agnoli, N. G. Apostol, P. Lacovig, S. Lizzit, D. Farías, et al., Unveiling the mechanisms leading to h 2 production promoted by water decomposition on epitaxial graphene at room temperature, ACS Nano 10 (4) (2016) 4543–4549. doi:10.1021/acsnano.6b00554.

[52] L. Marcinauskas, M. Silinskas, A. Grigonis, Influence of standoff distance on the structure and properties of carbon coatings deposited by atmospheric plasma jet, Appl. Surf. Sci. 257 (7) (2011) 2694–2699. doi:10.1016/j.apsusc.2010.10.047.
URL http://www.sciencedirect.com/science/article/pii/S0169433210014133

[53] C. Gong, M. Acik, R. M. Abolfath, Y. Chabal, K. Cho, Graphitization of Graphene Oxide with Ethanol during Thermal Reduction, J. Phys. Chem. C 116 (18) (2012) 9969–9979. doi:10.1021/jp212584t.
URL https://doi.org/10.1021/jp212584t